

CVD-Assisted Synthesis of 2D Layered MoSe₂ on Mo Foil and Low Frequency Raman Scattering of Its Exfoliated Few-Layer Nanosheets on CaF₂ Substrates

Rajashree Konar,[†] Bharathi Rajeswaran,[†] Atanu Paul, Eti Teblum, Hagit Aviv, Ilana Perelshtein, Ilya Grinberg,* Yaakov Raphael Tischler,* and Gilbert Daniel Nessim*



Cite This: *ACS Omega* 2022, 7, 4121–4134



Read Online

ACCESS |



Metrics & More

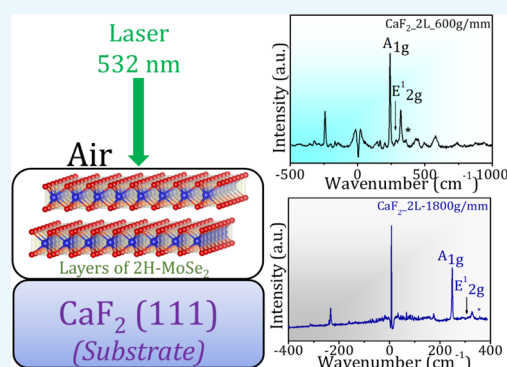


Article Recommendations



Supporting Information

ABSTRACT: Transition-metal dichalcogenides (TMDCs) are unique layered materials with exotic properties. So, examining their structures holds tremendous importance. 2H-MoSe₂ (analogous to MoS₂; Gr. 6 TMDC) is a crucial optoelectronic material studied extensively using Raman spectroscopy. In this regard, low-frequency Raman (LFR) spectroscopy can probe this material's structure as it reveals distinct vibration modes. Here, we focus on understanding the microstructural evolution of different 2H-MoSe₂ morphologies and their layers using LFR scattering. We grew phase-pure 2H-MoSe₂ (with variable microstructures) directly on a Mo foil using a two-furnace ambient-pressure chemical vapor deposition (CVD) system by carefully controlling the process parameters. We analyzed the layers of exfoliated flakes after ultrasonication and drop-cast 2H-MoSe₂ of different layer thicknesses by choosing different concentrations of 2H-MoSe₂ solutions. Further detailed analyses of the respective LFR regions confirm the presence of newly identified Raman signals for the 2H-MoSe₂ nanosheets drop-cast on Raman-grade CaF₂. Our results show that CaF₂ is an appropriate Raman-enhancing substrate compared to Si/SiO₂ as it presents new LFR modes of 2H-MoSe₂. Therefore, CaF₂ substrates are a promising medium to characterize in detail other TMDCs using LFR spectroscopy.



INTRODUCTION

Graphene isolation in 2004 initiated the research era into layer separation and subsequent analyses of various two-dimensional (2D) materials containing exciting properties.¹ Among the widely growing 2D layered materials, transition-metal dichalcogenides (TMDCs) have attracted significant attention. This family of materials possesses a sizable band gap, and several reports indicate that they could be suitable as active layers in logic electronics and optoelectronics in addition to electrode components in a variety of energy-related applications. Layered TMDCs have the generic formula MX₂, where M stands for metal and X represents a chalcogen. Their interatomic interactions within each layer are covalent. All of these individual layers are held together by weak van der Waals (vdW) forces (for example, in MoS₂, MoSe₂, WS₂, WSe₂, WTe₂, NbSe₂, etc.), just as in graphene.² These interlayer vdW forces are often responsible for structural anisotropy and cleaving of the layers.³ The vdW forces across the layers become more vital as we move down the group toward transition-metal tellurides than the transition-metal sulfides or selenides.

Understanding the fundamentals in the layer-stacking present in various 2D TMDCs is critical to producing new structured materials for different optoelectronic devices. Such devices are usually based on multiple structures combining

several identical or different 2D layers with varying relative orientations. The characterization of these 2D layered TMDCs is generally performed with electron microscopy, atomic force microscopy, and optical spectroscopy methods. Among all of these methods, Raman spectroscopy holds particular importance due to its simplicity and nondestructive nature toward the structural investigation of TMDCs, similar to what is done for many carbon-based systems, such as in carbon nanotubes and graphene.⁴ Raman spectroscopy studies on TMDCs such as MoS₂ have successfully identified low-frequency shear modes (SMs) and layer-breathing modes (LBMs) in addition to clarifying their corresponding stacking polytypes. These modes occur close in energy to the Rayleigh line and can only be observed using purpose-built filters.^{5–8} The SMs and LBMs show a characteristic blue shift and red shift, respectively, as the layer number increases from monolayer to two layers till the bulk material. For group 6 TMDCs, there are many

Received: October 10, 2021

Accepted: January 4, 2022

Published: January 24, 2022



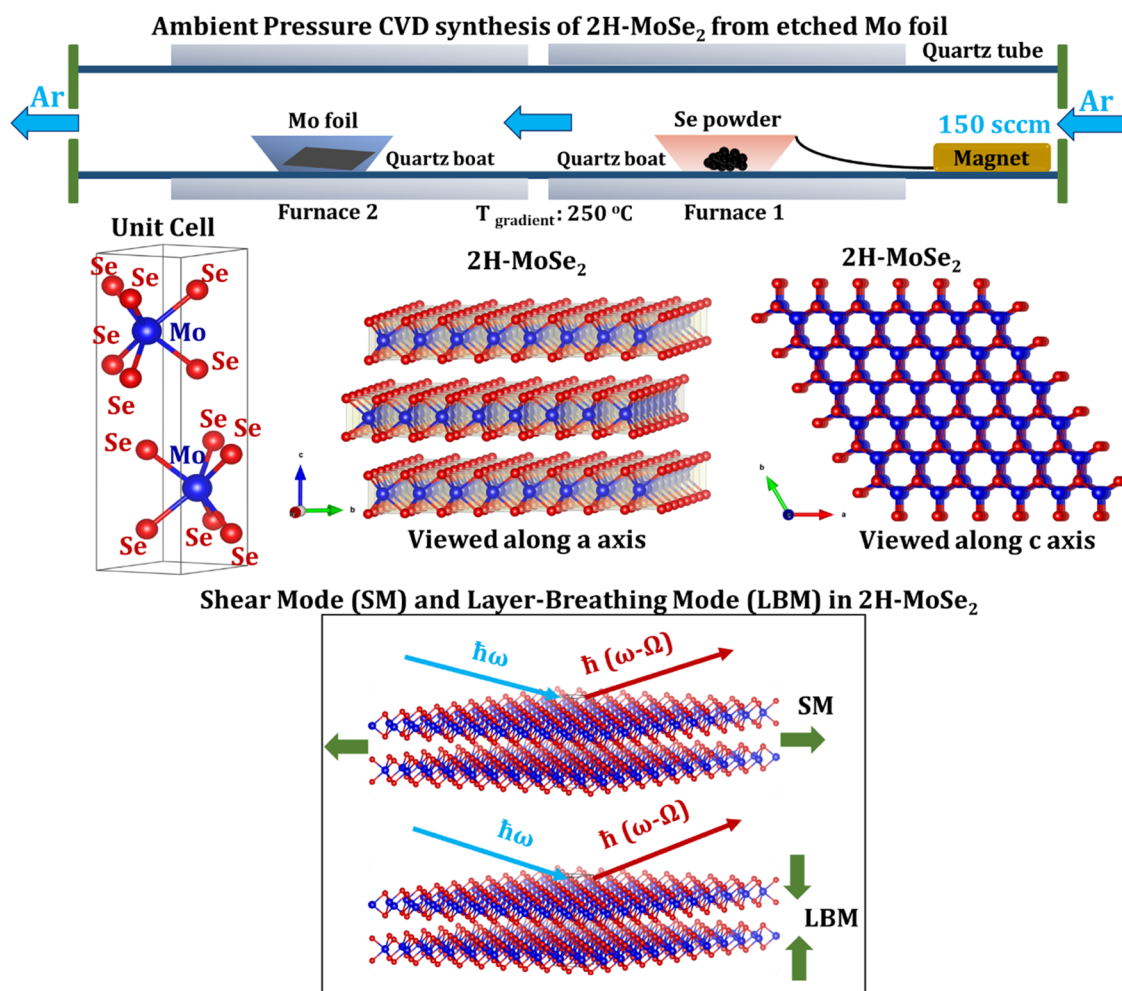


Figure 1. Schematic for ambient-pressure chemical vapor deposition (CVD) synthesis of 2H-MoSe₂ starting from a Mo foil and Se powder. The Mo foil is etched with different HCl strengths (giving rise to four different morphologies with varying strengths of HCl). Furnace 1 is set at 650 °C, and furnace 2 is set at 900 °C (maintaining a temperature gradient of 250 °C). A 2 cm × 2 cm Mo foil and 1.5 g of Se are shown in the schematic. The flow of Ar gas is set to 150 sccm. A ball and stick representation of the 2H variant of 2H-MoSe₂ is demonstrated. Red balls indicate Se, and blue balls show Mo in the unit cell drawn beside (where $a = 3.288$ Å and $c = 12.91$ Å). The structures are visualized along the a -axis and c -axis. A representation of the shear mode (SM) and the layer-breathing mode (LBM) of 2H-MoSe₂ is also shown.

reported polymorphs, some of them being 3R (R = rhombohedral), 2H (H = hexagonal), 1T, and 1T' (T = trigonal). The 2H phase is the most common and thermodynamically stable polytype of group 6 TMDC, where each unit cell is composed of two trigonal prisms of adjacent layers. Figure 1 shows the basic 2H polymorph of MoSe₂ (the unit cell of which is identical to the final product we synthesized).

Raman analyses of commercially purchased MoSe₂ and bottom-up CVD-grown MoSe₂ focus on its high wavenumber Raman modes. The recent reports on Raman mapping of low wavenumber modes shed light on several factors responsible for the inherent behavior of the MoSe₂. Some prominent characteristics, such as layer numbers, stacking, relative orientations, twisting angles, grain boundaries, etc., were established.⁹ These studies have successfully determined whether we can easily integrate the exfoliated or as-grown MoSe₂ layers into electronic devices. Low-frequency Raman (LFR) peaks around 50 cm⁻¹ provide essential information on the SMs and LBMs associated with in-plane and out-of-plane interlayer vibrations. The LBM, being an out-of-plane vibration mode, fluctuates as a function of layer number.¹⁰ Identifying

such modes provides the most sensitive measurements of the vdW interactions between layers in various stacked 2D crystals with differences in the number of layers or phases.⁹ Moreover, LFR spectroscopy has also been recently used to reveal the relationship between interfacial coupling and stacking patterns in twisted multilayer graphene, a study which is extended to analyzing the most stable stacking configurations, 2H (or AA') and 3R (or AB), in bilayers and even more complex 2H-2H, 2H-3R, and 3R-3R stackings in trilayers of MoSe₂ of the previous reports on the fingerprint regions/modes of MoSe₂.¹¹

From the literature, the choice of substrates significantly impacts the clarity and information of the Raman signals. A suitable substrate should not have Raman modes in the frequency region of interest and should exhibit a low background and not mask the layers' excitation. Therefore, the use of dielectric materials as active substrates for Raman spectroscopy is based on those substrates being optically transparent without a feature in their Raman spectrum to avoid overlapping. These constraints reduced the suitability of dielectrics to silicon dioxide (SiO₂), calcium fluoride (CaF₂), or aluminum oxide (Al₂O₃) crystals. So, epitaxially grown and crystalline Raman-grade CaF₂ is gaining attention toward a

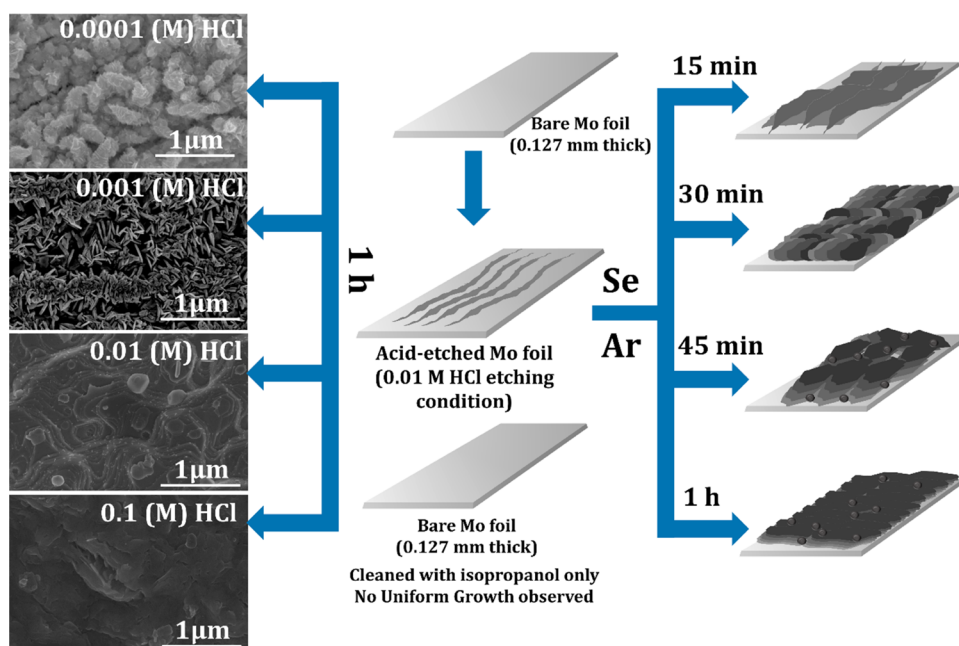


Figure 2. Evolution in the morphology (starting from 15 min up to 1 h of total reaction time) of bulk 2H-MoSe₂ grown directly on the Mo foil using only the Mo foil and elemental Se as the precursors in the presence of Ar as the carrier gas (images on the left show variations in the morphology due to acid-etching (starting from 0.0001 to 0.1 M HCl) of the Mo foil surface).

practical choice for Raman spectroscopic measurements.¹² CaF₂ has a favorable combination of high dielectric constant ($\epsilon = 8.43$), extremely wide band gap ($E_g = 12.1$ eV), highly effective carrier mass ($m^* = 1.0m_0$), and also insulating properties.¹³ It shows a signal only at 320 cm⁻¹, indicating that the background noise obtained from it is minimal compared to that from other dielectrics mentioned before. This substrate is also able to solve the fragile Raman intensity (resulting in low signal-to-noise ratios). Such signal enhancement is favorable for materials currently used as optical windows mainly because of their refractive indices in their transparency regions. Previous studies on 2D layered TMDCs (especially MoSe₂) showed a lot of information in the Raman spectra when these as-purchased materials were both mechanically/chemically exfoliated and then placed on commonly used substrates such as Si or Si/SiO₂.¹⁴ Our studies probed the substrate interference effect on the final Raman spectra and the quality of the obtained information, especially at frequencies starting typically from 50 to 200 cm⁻¹.

Many LFR studies of TMDCs show that MoSe₂ is a promising candidate comparable to its disulfide analogue for a device (given its narrower band gap of 1.5 eV with high mobility).^{15–17} Although reports on MoSe₂ are available, the LFR measurements have mainly been carried out on commercially purchased 2H-MoSe₂ or on layers grown directly on Si/SiO₂ substrates (where the substrate itself is a suitable dielectric for LFR measurements).¹⁸ In most of the as-synthesized 2H-MoSe₂ polymorphs, the syntheses were done in conjunction with (a) solid-state mixing of precursors (i.e., MoO₃ powder and Se powder) in a quartz ampoule and then hermetically sealed to be heated continuously for long hours, or (b) reacting MoO₃ in the form of a thin-film sputtered or deposited on the exposed surface of the Si/SiO₂ substrate in the presence of a reducing atmosphere before being reacted with Se vapor (with the reactions performed in chemical vapor deposition (CVD) or physical vapor deposition (PVD)

systems).¹⁹ In this context, we must mention that the microstructural evolution and the separation of the exfoliated layers of 2H-MoSe₂ synthesized from a Mo foil and elemental Se as the precursor using an atmospheric pressure two-furnace CVD system is not yet studied. Many reports focus on mechanical exfoliation from bulk as-purchased MoSe₂ crystals for LFR analyses.^{20,21} Often, this method suffers from improper layer separation and low yield. A gold-assisted mechanical exfoliation was pursued as an extension of such exfoliation.²² This is why, as a subgroup of top-down techniques, liquid-phase exfoliation (or LPE) is widely used as an effective method for proper layer separation.

Here, we report the successful separation of large-area layers or flakes from bulk 2H-MoSe₂ synthesized on a Mo foil (using the rapid thermal annealing–slow cooling technique, as shown in Figure 1). We used this procedure to grow 2D few-layered TMDCs directly on metal foils (such as WSe₂ on a W foil).^{23–25} To the best of our knowledge, we also provide a first-time report on the suitable etching procedure by analyzing the synthetic strategy that helped us grow a phase-pure 2H variant of MoSe₂ on a Mo foil without using H₂ reduction or any other reducing precursor. This particular variable acid-etching technique allows us to observe a systematic growth evolution based on its microstructure as observed from scanning electron microscopy measurements. We show good layer separation from two layers (L) up to 10 L by selecting appropriate low-boiling solvents for exfoliation.²⁶ Since finding a suitable substrate for Raman studies is always challenging, we base our analysis on correctly identifying a substrate with minimum background interference. This provides significant insights into the otherwise unknown modes or enhancements that were not reported previously from the drop-cast flakes from the bulk MoSe₂ samples (either grown from MoO₃ powder/Se powder using CVD or from MoO₃ sputtered on Si/SiO₂ and then selenized). To analyze the LFR signals from our sample, we carried out this study to compare two different

substrates, namely, Si/SiO₂ and CaF₂. The outcome of our research is twofold. We established a growth mechanism on variable acid-etching of the Mo foil surface, leading to control over the final microstructure. We also showed that the Raman-grade CaF₂ substrate is a promising choice to identify and locate some additional hybrid modes of exfoliated CVD-grown 2H-MoSe₂.

RESULTS AND DISCUSSION

Thermodynamically Stable Phase (2H-MoSe₂) Formation Mechanism on a Mo Foil (with Variable Acid-Etching of the Mo Surface). The reaction between the Mo foil and elemental Se is carried out in a two-furnace ambient-pressure chemical vapor deposition (AP-CVD) system where a 1 cm × 1 cm Mo foil is placed in a quartz boat in furnace F2, and elemental Se is placed in a quartz boat in F1. The temperatures at F1 (Se side) and F2 (Mo foil side) were increased to 650 and 900 °C, respectively (as shown in Figure 1). Following our previous work on tungsten diselenide (2H-WSe₂), we performed an exhaustive refinement of our reaction parameters to observe the evolution in the morphology of the bulk 2H-MoSe₂.²³

The nucleation occurred within 15 min of reaction between the Mo foil and elemental Se, which eventually progressed to uniformly sized flakes at 1 h. The reaction time of 1 h was optimized because we observed an almost complete reaction of the Mo foil with the elemental Se precursor, leading to a precise arrangement in its overall flake organization as suggested by the layered formation of MoSe₂ on the exposed Mo foil surface (Figure 2).

We found that the process is scalable as we tested bigger batches using Mo foils of size 4 cm × 4 cm, 2 cm × 6 cm, and 2 cm × 8 cm (thickness 0.127 mm). For the bigger-sized Mo foils (i.e., 2 cm × 2 cm, 4 cm × 4 cm, and 2 cm × 6 cm), we used 2.5 g of elemental Se for the growth and the 2 cm × 8 cm Mo foil; we performed the same experiment using 2.6 g of elemental Se. In both cases, the greater amount of Se loading formed a similar and uniform morphology.

The CVD-assisted synthesis of 2H-MoSe₂ led to a phase-pure material with a layered sheetlike structure (reaction mechanism shown in Figure 2 and microstructural growth progression of bulk MoSe₂ shown in Supporting Information Figure S1a–d). The whole optimization procedure is also shown in Supporting Information Figure S1, indicating that the best exfoliable layers were obtained only from a 0.01 M etched sample. High-resolution scanning electron microscopy (HRSEM) images of optimized 2H-MoSe₂ from different reaction times help us probe into the microstructural evolution of the few-layered flakes on the Mo foil's surface. As the reaction progressed from 30 min onward, the HRSEM images in Supporting Information Figure S1b suggest an underlying secondary growth in the form of tiny particles in addition to the formation of contoured layers of 2H-MoSe₂ throughout the Mo foil.

Role of Surface Etching of Molybdenum Foils in Preparing Phase-Pure Molybdenum Selenide (2H-MoSe₂) with Varying Morphologies. The effects of surface etching are evident in the MoSe₂ synthesis on the Mo foil using elemental precursors in the presence of inert carrier gas. We have adopted the acid-etching technique to remove the surface oxide layer on the Mo foil. This method further initiated random nucleation points on the foil's surface, which led to the final 2H-MoSe₂ formation. The acid-etched surface

of the foil acts as the primary and secondary nucleation sites for inducing the initial reaction between the Se vapor and the Mo surface.²³ We increased the strength of the acid by 10 times in each case to observe if there is any variation in the surface microstructure. This was done for the following reasons: (a) we did not see any difference in growth or changes in the morphology when the acid strength was increased from 2 times to 8 times; (b) the morphology showed a significant modification from fernlike structures to large lateral-sized 2D sheetlike and platelike flakes, and (c) based on the variable microstructures, we studied the respective exfoliation parameters to understand how we could easily separate individual flakes in addition to observing the number of layers after drop-casting. Our observations assured that changing the acid strength leads to significant changes in the surface morphology. The HRSEM images of surface-etched Mo foils in different strengths of HCl are shown in Supporting Information Figure S2a–d. The reaction between the Mo foil and HCl is also shown in equation (2) after Supporting Information Figure S2.

Identifying the Effect of Surface Etching of Molybdenum Foils on Forming Different Microstructures of 2H-MoSe₂. To understand the effect of acid-etching on the formation of the final microstructure, we performed an exhaustive synthesis parameter variation. We tuned the microstructure of the MoSe₂ using several approaches such as variations in the gradient temperature (i.e., the temperature difference between the two furnaces), type of inert gas used (Ar or He), amount of Se loading, and surface etching. Out of all of the strategies we tried, only surface etching was responsive toward forming a variable microstructure (keeping all of the other variables constant). Based on the strength of the acid used, we checked the microstructure of the bare etched Mo foil. The foils etched with dilute acid show some roughness on the surface. This means that the nucleation sites formed for the cases of dilute acid-etching are comparatively less [as indicated by Supporting Information Figure S3(1,2)]. It indicates that the incoming Se vapor interacted with the exposed areas to form smaller lateral-sized flakes or nanosheets. The tendency toward a greater surface roughness is evident in the case of higher acid-strength etching [as indicated by Figure S3(3,4)]. It also led to a trend toward the accumulation and fusing of the individual 2D sheets growing on the Mo surface (which makes the vdW forces stronger in the case of the 0.1 M HCl etched sample). The same increase in vdW forces between the flakes is also noticed in the case of the other two samples (0.0001 and 0.001 M etched), which are difficult to exfoliate as well. However, the most optimized sample uses 0.01 M HCl as the 2D sheets can be easily exfoliated using LPE. The fernlike, leaflike, and platelike microstructures can be exfoliated but only with very high exfoliation times and higher sonication frequencies.

We also checked the Se loading effect on the final microstructure. It seems that the morphology is highly dependent on the surface etching as increasing/decreasing the loading of Se by 0.25 g results in identical microstructures. In Supporting Information Figure S4a–l, we show the growth trend of different MoSe₂ morphologies under different etching conditions.

So, the acid-etching of the Mo foil at different concentrations of HCl led to fernlike MoSe₂ (0.0001 M HCl), leaflike sheets of MoSe₂ (0.001 M HCl), and platelike MoSe₂ (0.1 M HCl) on the Mo foil surface (additional HRSEM imaging of

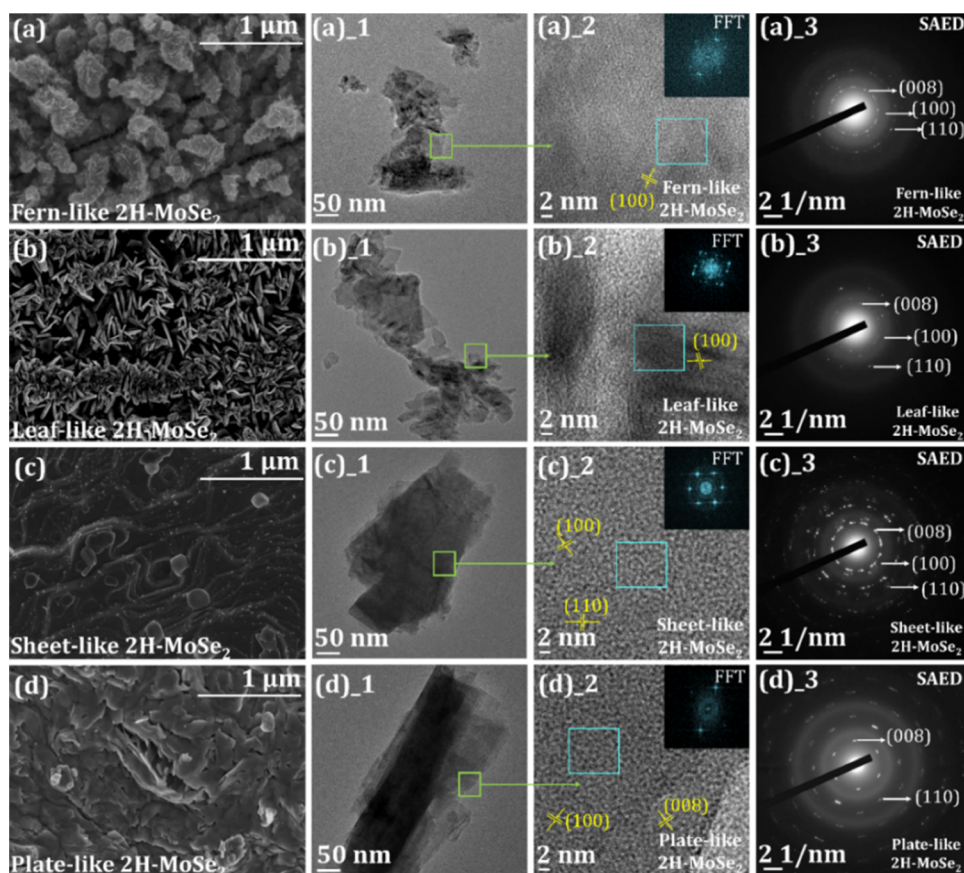


Figure 3. Evolution in the morphology of 2H-MoSe₂ concerning variable etching conditions using HCl (starting from etching of the pristine Mo foil in (a) 0.0001 M (fernlike), (b) 0.001 M (leaflike), (c) 0.01 M (sheetlike), and (d) 0.1 M ([platelike) HCl solutions). All of the visible interlayer fringes are shown in each high-resolution transmission electron microscopy (HRTEM) image corresponding to the respective morphologies.

bulk growth progression of each microstructure is shown in Supporting Information Figure S4 and discussed later in Figure 3 in the next paragraph).

Optimized 2H-MoSe₂ layers have a characteristic hexagonal-shaped holelike shape between specific numbers of layers (in the case of etching with 0.01 M HCl). We can assume that the acid-etching procedure, in all cases, is responsible for the variation in nucleation and growth. Further investigation into the exfoliated material (optimized 2H-MoSe₂; 0.01 M HCl etching of the Mo foil surface) confirms its physical characteristics. The bright-field transmission electron microscopy (BF-TEM) measurements in Supporting Information Figure S5(a₁,a₂) indicate the distinct layers present in the material after successful exfoliation with ethanol and isopropanol as solvents. The fast Fourier transforms (FFTs) obtained from the high-resolution transmission electron microscopy (HRTEM) and the very distinct assignment of the individual planes in the selected area diffraction (SAED) pattern are all indicative of a consistent morphology, layers, and quality of the material after exfoliation [Supporting Information Figure S5(a₃–a₆)]. A closer inspection into the high-magnification HRSEM images [Supporting Information Figure S5(b₁–b₃)] confirms the layer-by-layer growth of the MoSe₂ on the Mo foil surface. We also performed the X-ray diffraction (XRD) analysis on the bulk and exfoliated MoSe₂, as shown in Supporting Information Figure S5(c₁). We indexed it to the 2H (hexagonal) phase of MoSe₂ (ICDD reference code: 00-029-0914) (with no excess Se or unreacted

Mo present in the material) as expected for the symmetry group $P6_3/mmc$. X-ray photoelectron spectroscopy (XPS) measurements of the as-exfoliated MoSe₂ sample again confirm the oxidation state and indicate the presence of only Mo and Se [as shown in Figure S5(c₂,c₃)]. The two well-defined peaks of Mo, i.e., Mo 3d_{5/2} and Mo 3d_{3/2} in the core level spectra at ~ 228.78 and ~ 231.90 eV, indicate the typical +4 oxidation state of Mo. In contrast, the deconvoluted doublet of Se, i.e., Se 3d_{5/2} and Se 3d_{3/2} at ~ 54.49 and ~ 55.35 eV, is also indicative of the -2 oxidation state of Se in 2H-MoSe₂.

We concluded from our experiments that every acid-etched Mo foil acts as a self-nucleating template for MoSe₂ growth. This behavior is often observed in solvothermal routes where different initial precursors can self-tailor nucleating points, further developing the final material.^{27,28} Figure 3 shows the high-resolution transmission electron microscopy (TEM) images for each microstructure. All of the selected area diffraction patterns (SAEDs) can be assigned to 2H-MoSe₂. The TEM images have comparatively thicker layers (than the layer variation studies on optimized MoSe₂) because each dispersion was prepared from 100 mg of each microstructure dispersed in 50 mL of ethanol. The drop-cast layers (≥ 2 drops) on the TEM grid has almost 10–12 sheets stacked on top of each other, as evident from the TEM images.

Additional microscopy measurements of optimized MoSe₂ [i.e., the HRTEM measurements and the fast Fourier transforms (IFFTs)] are shown in Supporting Information Figures S5 and S6. The bulk HRSEM image of MoSe₂

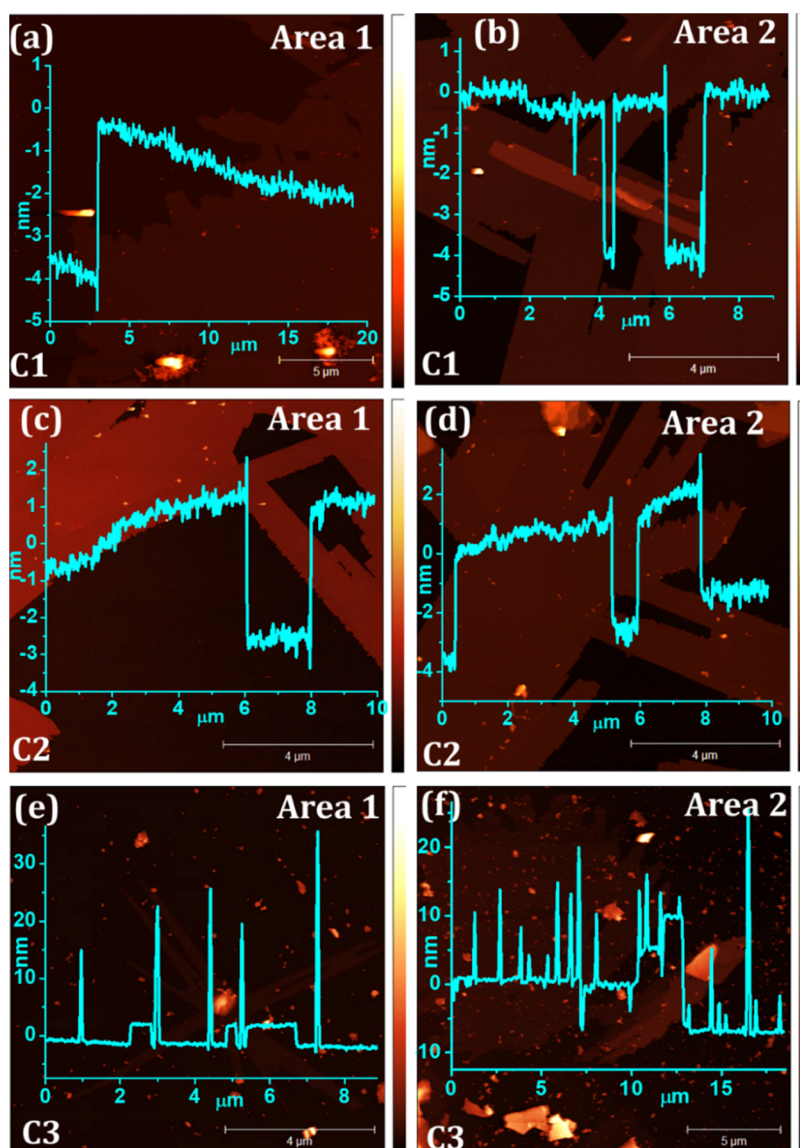


Figure 4. Change in the total number of layers in exfoliated 2H-MoSe₂ grown on the Mo foil at 1 h of reaction between the Mo foil (etched with 0.01 M HCl) and elemental Se to the total number of droplets of the ethanol-based solution of the exfoliated TMDC starting from (a, b) ~2–3 L of 2H-MoSe₂ from concentration 1 (C1) of exfoliated ethanol-based dispersion of 2H-MoSe₂ (height profile: $\sim 2.7 \pm 0.3$ nm), (c, d) ~5–7 L from concentration 1 (C2) of exfoliated ethanol-based dispersion of 2H-MoSe₂ (height profile: $\sim 3.54 \pm 0.3$ nm), and (e, f) ~10–15 L from concentration 1 (C3) of exfoliated ethanol-based dispersion of 2H-MoSe₂ (height profile: $\sim 14.8 \pm 0.3$ nm).

synthesized at 1 h of reaction, its complete area mapping, energy-dispersive X-ray spectroscopy (EDS) profiling, and additional HRTEM imaging with corresponding FFTs from different regions of the exfoliated MoSe₂ layers (provided in Supporting Information Figure S6a,b,b_1,b_2,b_3,b_4,c,d,e) all agree with the formation of the 2H phase of MoSe₂). In addition, we did not observe any unreacted Mo and Se in all of the microstructures.

Liquid-Phase Exfoliation Optimization for Molybdenum Selenides (2H-MoSe₂) with Varying Morphologies (in Comparison to Micromechanical Exfoliation and Deposition). Micromechanical exfoliation is one of the most popular choices for separating and depositing any layered TMDC on a suitable substrate (such as sapphire, Si/SiO₂) for further measurements by AFM. This can help identify the possible number of layers (in our case for 2H-MoSe₂). However, it is possible that the MoSe₂ layers might have

incomplete separation during harsh mechanical exfoliation via scotch tape (as indicated in Supporting Information Figure S7a,b). For this reason, we use liquid-phase exfoliation (LPE) employing low-boiling point solvents such as ethanol and isopropanol for further measurements via AFM.²⁶ The Si/SiO₂ substrates were cleaned before MoSe₂ nanosheet deposition using a standard cleaning procedure.²⁹ Post exfoliation, we also noticed a similarity of the layered large-area flakes generated from the 2H-MoSe₂ synthesized under two etching conditions (i.e., 0.01 M HCl and 0.1 M HCl). The only difference lies in the total sonication time of the variable morphologies.

For all of the variable morphologies of 2H-MoSe₂, we optimized the necessary exfoliation parameters. The large sheets of 2H-MoSe₂ synthesized at 1 h of reaction between the Mo foil and Se powder (0.01 M HCl) were the easiest to exfoliate. The consistency of the layers and the ease of exfoliation were driving factors for us to continue further LFR

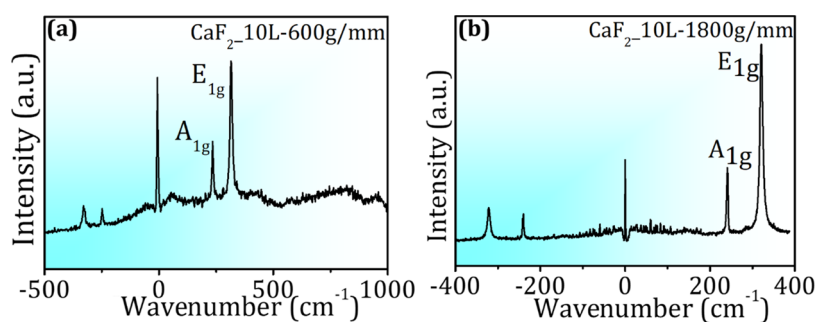


Figure 5. Low-frequency Raman spectra of 10 layers of 2H-MoSe₂ on CaF₂ using two different gratings (600 and 1800 grooves/mm). Supporting Information Figure S11a,b contains the optical white light images of the flakes at two different magnifications (50× and 100×).

measurements with that particular set. In addition, each of the morphologies analyzed under the TEM revealed the formation of a phase-pure 2H-MoSe₂ only, indicating that our synthetic procedure is highly reproducible (as per Figure 3a–d shown previously). Although we did image the other morphologies of 2H-MoSe₂ under the TEM, the exfoliation process of different microstructures was prolonged. It took a long time (>4 h, with breaks in between) of harsher exfoliation conditions to produce the final suspension in ethanol and isopropanol solutions for MoSe₂ with fernlike and leaflike morphologies. Therefore, according to the TEM images, we can correlate the morphological differences to the variable length of the nanosheets (ranging from about 30 nm for etching with 0.0001 M HCl to about 2 μm for etching with 0.1 M HCl). The extent of exfoliation can also be argued on the strength of the interlayer van der Waals (vdW) forces, which seem to be the least in the case of the microstructure of 2H-MoSe₂ obtained from 0.01 M HCl etching of the Mo foil surface (i.e., the large-area nanosheet-like 2H-MoSe₂). The exfoliation parameters of each morphology are highlighted, and the respective thickness of the drop-cast layers is shown via AFM of every individual microstructure in Supporting Information Figure S8a–d.

Liquid-Phase Exfoliation (LPE) and Drop-Casting from Bulk 2H-MoSe₂ (Synthesized at 1 h of Reaction between the Mo Foil (Etched with 0.01 M HCl) and Elemental Se). We wanted to understand the variation of the number of layers after the liquid-phase exfoliation of 2H-MoSe₂ (optimized with 0.01 M HCl etching of the Mo foil surface) from the bulk. To study the effect of modulating the total number of layers, we extracted 0.5, 5, and 10 mg of the 2H-MoSe₂ powder from the Mo foil surface in 20 mL of ethanol. We sonicated this material at different times and obtained a uniform and homogeneous dispersion at 60 min, 80 kHz, and 100% power. We studied this dispersion similarly to what we did in our previous reports.^{23,24} We also examined the stability of the 2H-MoSe₂ dispersions in ethanol. We understand that this material's dispersions are very stable and highly homogeneous (almost tending toward a solution-like dispersion, as shown in Supporting Information Figure S9). We drop-cast each of the different concentrations of MoSe₂ in ethanol (1 drop for each concentration) onto both Si/SiO₂ substrates and CaF₂ substrates and dried them under ambient conditions. Figure 4 shows the total number of MoSe₂ layers we obtained in each concentration after being drop-cast onto Si/SiO₂. We used Si/SiO₂ explicitly for our atomic force microscopy (AFM) measurements because the contrast obtained for CaF₂ was relatively low and could not be properly profiled using the AFM probe. The subsequent dispersions on

CaF₂ were probed mainly using optical microscopy images from the in-built camera of the Raman spectrometer, which helped us to understand the layer variation and the expected number of layers that we can obtain if we follow the same LPE procedure for drop-casting the MoSe₂ dispersion onto the CaF₂ substrates.

For the drop-cast flakes of 2H-MoSe₂ on Si/SiO₂ substrates, we observed that the corresponding height profiles (as per Figure 4 a,b) were 2.7 ± 0.3 nm (indicating about 2–3 L of MoSe₂), (Figure 4c,d) $\sim 3.54 \pm 0.3$ nm (indicating about 5–7 L of MoSe₂), and (Figure 4e,f) 14.8 ± 0.3 nm (indicating about 10 L of MoSe₂). The height profiles of the drop-cast MoSe₂ flakes (from each concentration, namely, C1, C2, and C3) were recorded from two different regions (area 1 and area 2 in all three cases) after ultrasonication, and an average of the height profiles was evaluated. Each of these drop-cast MoSe₂ flake sets was further analyzed by low-frequency Raman (LFR) spectroscopy to observe if new LFR peaks appear in the case of both Si/SiO₂ and CaF₂ substrates.

Low-Frequency Raman (LFR) Spectra of >10 L 2H-MoSe₂ (Synthesized at 1 h of Reaction between the Mo Foil (Etched with 0.01 M HCl) and Elemental Se) on CaF₂. Our studies probed the substrate interference effect on the final Raman spectra and the quality of the obtained information, especially at frequencies from 50 to 200 cm⁻¹. The justification for using CaF₂ as a substrate in our experiments lies in a few factors. For example, the influence of the substrate on the Raman intensity of graphene in a previous work shows the Raman scattering efficiency of graphene on CaF₂. It strongly modulated the Raman intensity in such a way that the signals and spectra obtained proved it a superior substrate for Raman measurements in contrast to Si/SiO₂.¹⁴ In other recently reported biological and organic samples' cases, CaF₂ was chosen for detection and analysis in infrared spectroscopy areas.³⁰ So, CaF₂ has proven to be an excellent choice for organic and biological films. It has a refractive index of about 1.422, close to that of water (and many organic materials).³⁰ Accordingly, it is expected that even if there are interference effects, they should be minimal and possibly negligible. Although CaF₂ displays a well pronounced Raman mode at 321 cm⁻¹, the energy gap of 12 eV is considerably higher than the visible photon's energy. This energy gap ensures that resonance effects will not play a role in Raman scattering, whereas we cannot neglect the corresponding resonance effect for Si (1.1 eV, infrared range).³⁰

As for SiO₂, there are reports on how it enhances the Raman response of graphene-based thin-film interference effect, depending on the thickness of the SiO₂ layer deposited on crystalline Si. The SiO₂ layer thickness should be fine-tuned to

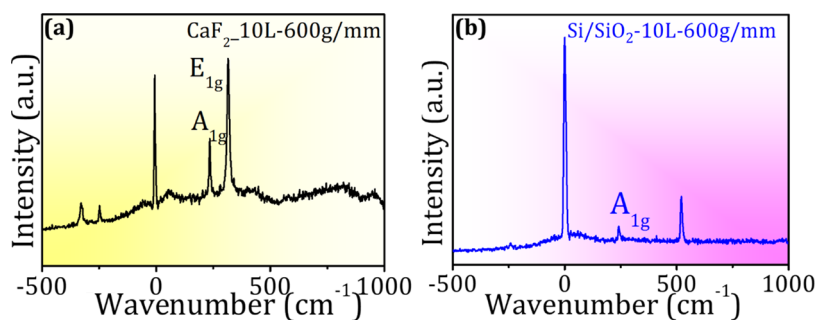


Figure 6. Low-frequency Raman of 10 L of MoSe₂ drop-cast on (a) CaF₂ and (b) Si/SiO₂ substrates. (Off-focus to probe A_{1g} and ¹E_{2g}).

achieve maximum enhancement at the Raman experiment's laser line. The thickness (T) is calculated from the following equation³⁰

$$T_n(\text{SiO}_2) = (2m - 1)\lambda/4 \quad (1)$$

where $m = 0, 1, 2, 3, \dots$ and n is the refractive index of SiO₂ at wavelength λ .

So, the LFR signal for TMDCs on CaF₂ should be significantly enhanced, leading to possible signals otherwise considered noise in some previous reports.⁹ We tried to determine whether the additional modes observed from our studies are due to layer variations in the drop-cast few-layered 2H-MoSe₂. By probing LFR, we have also demonstrated the usefulness of studying these modes. These low-frequency modes occur due to the planes' relative motions, either perpendicular or parallel to the atomic layers, and can thus help characterize 2D materials. Additional peaks can be observed in the LFR region (<50 cm⁻¹).

Figure 5 shows the LFR spectra of layers of MoSe₂ measured on the Raman-grade CaF₂ substrate. The Raman spectrum of CaF₂ (Raman grade) is provided in Supporting Information Figure S10a, and the Raman spectrum of Si/SiO₂ is also shown in Supporting Information Figure S10b. The Raman-grade CaF₂ has flat Raman spectra except for only one peak at 320 cm⁻¹. This is important because, in MoSe₂ layers, the peaks are seen between 10 and 350 cm⁻¹. To identify the modes of 2H-MoSe₂, we proposed using CaF₂ without an interfering background Raman spectrum.

We identified ~10–15 layers (L) of 2H-MoSe₂ from AFM measurements on the Si/SiO₂ substrate. For the sake of reference, we denote this as 10 L in general to describe the Raman measurements. We show the white light imaging on the sample and Raman experiments with the laser focusing the flakes in Figure 5. We took images at two different magnifications and the spectra at two different resolutions with two different gratings (600 and 1800 g/mm). We see from our measurements that the LFR regions of MoSe₂ agree with the most common and thermodynamically stable polytype having a 2H configuration. For a 10 L 2H-MoSe₂, we identified the following peaks: 239 and 287 cm⁻¹. We observe similar peaks with two gratings, namely, 600 and 1800 grooves/mm. The results are consistent with the available reports. Typically, the peak at 287 cm⁻¹ corresponds to E_{1g} and 239 cm⁻¹ to A_{1g}. We similarly compare the Raman spectrum of 2H-MoSe₂ to the same drop-cast number of layers on the Si/SiO₂ substrate.

Effect of the Substrate on the LFR Spectra of 2H-MoSe₂ (Synthesized at 1 h of Reaction between the Mo Foil (Etched with 0.01 M HCl) and Elemental Se): A Comparison between CaF₂ and Si/SiO₂ Substrates for

Raman Measurements. Figure 6a shows the Raman spectrum of 10 L MoSe₂ drop-cast on CaF₂ substrates, and Figure 6b shows the same drop-cast on Si/SiO₂ substrates. Although fingerprint peaks of MoSe₂ deposited on Si/SiO₂ appeared at 241 cm⁻¹ corresponding to A_{1g}, the intensity of other MoSe₂ peaks was either less in contrast or not present. This can be attributed to the Si/SiO₂ substrate, as the highly intense Si (520 cm⁻¹) peak engulfs the other details of the 10 L MoSe₂. The flakes deposited on CaF₂ contain all of the fingerprint information of MoSe₂, especially in the lower frequency regions of MoSe₂, which the Si/SiO₂ substrate could not resolve. Therefore, we can enhance the resolution of LFR peaks simply using the right choice of substrates.^{9,31–33} Previous Raman signal enhancement studies suggest various research avenues, such as tip-enhanced Raman spectroscopy (TERS), interference-enhanced Raman spectroscopy (IERS), etc., to efficiently use the incident beam intensity by choosing appropriate substrates.³⁴ Here, we compare the effect of two dielectric substrates (namely, CaF₂ and Si/SiO₂) to obtain the complete spectral features of MoSe₂.

Figure 6 also shows the difference in the LFR spectrum of MoSe₂ between (a) CaF₂ and (b) Si/SiO₂ substrates. The Raman spectrum of 10 L MoSe₂ on CaF₂ showed prominent MoSe₂ peaks corresponding to ¹E_{2g} and A_{1g} modes, whereas the same 10 L MoSe₂ drop-cast on Si/SiO₂ substrates exhibited a weak A_{1g} peak characteristic to MoSe₂. Such behavior can be attributed to the CaF₂ substrate nature, compared with other substrates, such as Si/SiO₂, as discussed by Gasparov et al.³¹ According to Gasparov et al., a substrate containing no Raman modes with low Raman background within the frequency range will not mask excitations coming from the film. They also show that the m -value, the slope of power vs incident laser intensity, is used to eliminate a non-Raman background's potential effect.³¹ This slope is the least for CaF₂ and lower than that of Si/SiO₂. We compare the laser power vs intensity of Raman-grade CaF₂ and Si/SiO₂ in Supporting Information Figure S11a,b, respectively. This normalization of the Raman intensity of a material of interest to known Raman reference will allow consistent Raman intensities. Spectral features of Raman-grade CaF₂ lie at 320 cm⁻¹ and that of Si/SiO₂ at 520 cm⁻¹, qualifying both substrates to be used for Raman measurements (but gives better clarity in the case of CaF₂ as per our measurements). Comparing the refractive indices of CaF₂, SiO₂, and MoSe₂ at the 532 nm laser line, i.e., 1.4354, 1.4607, and 4.7995, respectively, the materials can be arranged in the increasing order of refractive indices: CaF₂ > SiO₂ > MoSe₂.

Effect of Layer Numbers on the Low-Frequency Raman Spectra of 2H-MoSe₂ (Synthesized at 1 h of

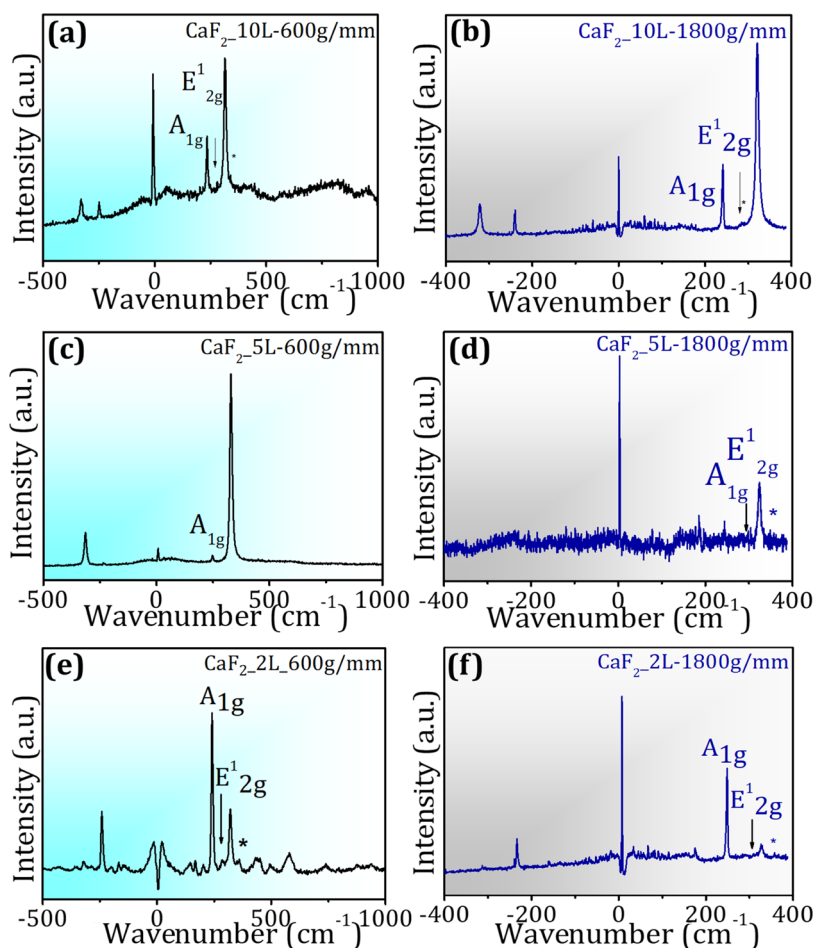


Figure 7. (a), (c), (e) Raman spectra for the different number of layers of MoSe₂ drop-cast on CaF₂ substrates using 600 g/mm; (b), (d), (f) different number of layers of MoSe₂ drop-cast on 1800 g/mm spectrometers (peak 350 cm⁻¹ is starred for clarity and measurement done off-focus to point at only two well-known characteristic modes A_{1g} and ¹E_{2g}).

Reaction between the Mo Foil (Etched with 0.01 M HCl) and Elemental Se). The in-plane vibration of metal–chalcogen atoms is recognized by an (E'/E_g/¹E_{2g}) Raman-active mode in the vicinity of 287 cm⁻¹. The out-of-plane (A'₁/A_{1g}) Raman-active mode is around 240 cm⁻¹. We generally observe these two modes in the Raman spectra of transition-metal dichalcogenides such as MoSe₂. Although the Raman peaks in transition-metal disulfides such as MoS₂ and WS₂ exhibit a shift in position with layer number allowing a monolayer and few-layers to be identified easily and quickly, in MoSe₂, these changes in frequency for different layer numbers are not very dramatic. The shift in peak can be as slight as the 1 cm⁻¹ shift in the A_{1g} peak from 2 to 3 L.¹⁸ For differentiating in the layer numbers (in the monolayer and bulk), another Raman peak at 350 cm⁻¹ is probed. This peak does not appear in monolayer and bulk. Hence, the absence of 350 cm⁻¹ is a confirmation of a monolayer or bulk. We also know that the in-plane mode exhibits a red shift, whereas the out-of-plane mode shows a blue shift, increasing the layer thickness. Figure 7 shows the effect of the number of layers on the LFR spectra of MoSe₂. The intensity of ¹E_{2g} is much lower than that of A_{1g} and is consistent with the available reports.³⁵ The corresponding high-resolution Raman spectra of 10, 5, and 2 L of MoSe₂ are shown in Figure 7b,d,e. In all of the samples, the in-plane metal–chalcogen vibration is present at 287 cm⁻¹ and the out-of-plane vibration at 240 cm⁻¹. They are labeled as ¹E_{2g} and

A_{1g}, respectively. In an earlier available report on MoSe₂ exfoliated on Si/SiO₂, a shear mode was identified at 20 cm⁻¹ for 2 L MoSe₂.³⁶ Similarly, in previous information, peaks in the spectrum are identified as containing a layer-breathing mode at 48 cm⁻¹ based on an LCM model fitted using the frequency of the bilayer Raman-active layer-breathing mode.^{36,37} In this work, we could not identify a shear mode at 20 cm⁻¹. Still, we could locate a few unreported peaks for 2 L MoSe₂ between 100 and 200 cm⁻¹ such as 145, 167, and 201 cm⁻¹, as shown in Figure 8 (corresponding optical images are shown in Supporting Information Figure S12a,b, and the effect of laser focus on 10 L MoSe₂ is shown in Supporting Information Figure S13). A similar identification of Raman modes for 1L 2H-WSe₂, from the literature, suggests peaks around 96, 116, 136, 157, 219, 239, and 249 cm⁻¹, similar to our inference in the case of MoSe₂.³⁸ In another report on 2H-MoTe₂, an unlabeled peak at 136 cm⁻¹ is assigned to be a second-order Raman mode.³⁹

As the number of layers decreased to 2 L, we identified more Raman modes. This can be due to the presence of surface defects.³⁵ We understand that most of these identified peaks for the corresponding layers at higher frequencies are consistent with previous literature reports. We have also identified a few Raman modes in addition to the A_{1g} and ¹E_{2g} modes. The identification of Raman modes of 2H-MoSe₂ reveals the presence of peaks such as 143, 162, and 198

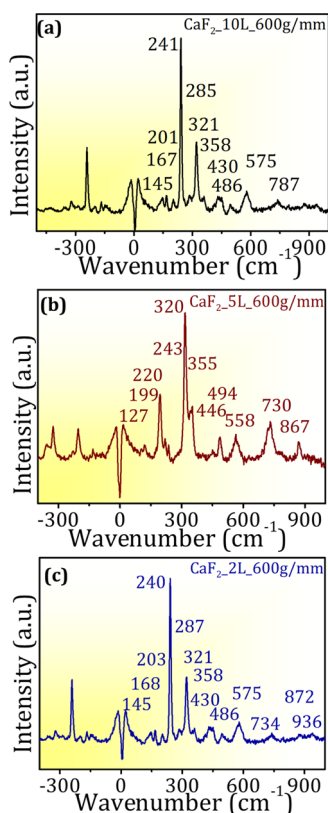


Figure 8. (a) 10 L, (b) 5 L, and (c) 2 L Raman spectra of 2H-MoSe₂ drop-cast on CaF₂ substrates using 600 g/mm (at laser focus).

cm⁻¹ and are ascribed to multiple-phonon scattering.⁴⁰ Simulated Raman spectra for the pristine system and the one with 25% vacancy concentration has shown a similar Raman spectrum in the report mentioned above.³⁵ Further characterization of the CaF₂ substrate (using XRD) is shown in Supporting Information Figure S14, and the photoluminescence spectra of 10 and 5 L MoSe₂ are shown in Supporting Information Figure S15a,b, respectively.

Figure 8 shows the Raman spectra of the three different samples (10, 5, and 2 L). These data are different from those in Figure 7 because the previous information is acquired at laser focus pointing only at A_{1g} and ¹E_{2g}. More specifically, we wanted to probe and identify the new modes of MoSe₂ that we observed at the three different regimes (region 1 or R1 (0–100 cm⁻¹), region 2 or R2 (100–200 cm⁻¹), region 3 or R3 (200–300 cm⁻¹), and region 4 or R4 (300–400 cm⁻¹). We observe a few typical peaks such as 145, 167, 200, 241, 285, and 355 cm⁻¹ for both 10 and 2 L samples. For the 5 L sample, there are peaks at 127, 199, 200, and 220 cm⁻¹ in addition to the well-known 243 and 355 cm⁻¹ peaks. The low-frequency peaks seen here can be ascribed to either multiphonon scattering or defect-related peaks.⁴⁰ The peak around ~220 cm⁻¹ can be assigned to a Se vacancy similar to the work of Zhao et al.,⁴¹ where the authors introduced different Se vacancies and studied the effect of the same in the Raman spectrum. So, we infer that the presence of 127 and 220 cm⁻¹ in the 5 L sample is related to the Se vacancy concentration. In the case of 10 and 2 L, there are peaks at ~145, 167, and 201 cm⁻¹ in the low-frequency region. This weak peak at 145 cm⁻¹ can be either associated with Se peaks found at 143 cm⁻¹ for trigonal selenium or can be a result of a two-photon process involving emission and absorption of a phonon as discussed by

McDonnell et al.⁴² Similarly, other weak peaks such as ~167 and 201 cm⁻¹ found in 10 and 2 L can be ascribed to a second-order Raman peak or a result of multiphonon scattering or can be related to defects.

To better comprehend the origin of the Raman modes of the 2, 5, and 10 L 2H-MoSe₂ system observed experimentally on the CaF₂ substrate, we first consider the (111) surface of CaF₂ and the MoSe₂ layers separately. Here, we focused on the 2 L MoSe₂ and used four formula units of CaF₂(111) surface formula units. The structures' energies are optimized with respect to ionic coordinates, and the optimized structures were used to calculate the Raman spectra with density functional perturbation theory. We show the calculated Raman intensity for the CaF₂(111) and 2 L of MoSe₂ in Figure 9a,b,

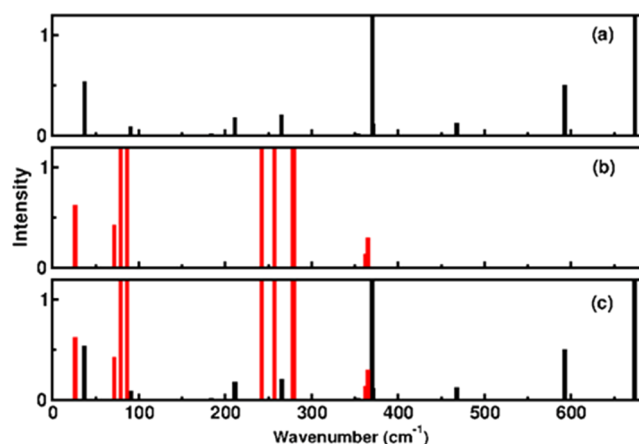


Figure 9. (Color online) Raman intensity for (a) the (111) surface of CaF₂ having four formula units, (b) two layers (2 L) of MoSe₂, (c) the (111) surface of CaF₂ (in black), and two layers of MoSe₂ (in red).

respectively. If the interactions between MoSe₂ and CaF₂ are negligible, the Raman spectrum of the MoSe₂ on the CaF₂ substrate should be a superposition of these two isolated systems' spectra. Therefore, we plot the Raman intensity for these two systems together in Figure 9c. Examination of Figure 9a shows that the Raman peaks of MoSe₂ are similar to the previously reported results obtained by density functional theory (DFT) calculations and experiments.⁴³ The Raman modes with significant intensity are situated in the 200–300 cm⁻¹ range. An examination of Figure 9b shows that for CaF₂(111), the Raman modes with a large intensity are above 300 cm⁻¹, as suggested by our experimental results.

Additionally, we observe peaks with a weak intensity from the CaF₂(111) surface below 300 cm⁻¹. The sum of the MoSe₂ and CaF₂ Raman spectra does not show the weak Raman peaks in the 100–250 cm⁻¹ range observed experimentally. This suggests that the experimental Raman peaks in these regions are not just from MoSe₂ but are most likely due to the interactions of the MoSe₂ with the CaF₂ surface or are related to vacancies and defects in MoSe₂.

CONCLUSIONS

We successfully synthesized phase-pure 2H-MoSe₂ on the Mo foil using a two-furnace CVD system. Our subsequent variable acid-etching of the Mo foil surface led to a variation in the bulk 2H-MoSe₂ morphology. Among all of the exfoliation procedures and morphologies, acid-etching with 0.01 M HCl

produced a nanosheet-like morphology with a proper layer separation on LPE in low-boiling solvents. Following the nanosheet phase characterization and microstructure, we separated the 2H-MoSe₂ flakes into 10-layer, 5-layer, and 2-layer MoSe₂ on CaF₂ and Si/SiO₂ substrates. We successfully identified well-defined enhanced Raman peaks on CaF₂ substrates previously unseen on the Si/SiO₂ substrates. In particular, we identified regular Raman modes such as ¹E_{2g} and A_{1g} in all of the samples. We also identified ~350 cm⁻¹ (^fB_{2g}), whose presence asserts that the material is neither monolayer nor bulk. For 2 L MoSe₂, we identified several weak peaks. This could be either due to multiphonon scattering or related to defects. Our measurements indicate that CaF₂ can serve as a 'Raman-enhancing' substrate to measure LFR scattering on 2H-MoSe₂. The strategic development of the various layered morphologies of the as-synthesized 2H-MoSe₂ on the Mo foil is a promising approach toward the CVD-based route. This particular synthetic approach and overall physical characterization using CaF₂ as a Raman-active substrate can similarly lead to the identification of new Raman fingerprints in other layered 2D TMDCs. We plan to pursue such measurements on other TMDC systems as an extension of this work.

EXPERIMENTAL SECTION

Synthesis of 2H-MoSe₂ on the Mo Foil. All reagents are used in as-purchased conditions (Alfa Aesar). We synthesized molybdenum diselenide (MoSe₂) using an ambient-pressure chemical vapor deposition (AP-CVD) system, composed of two furnaces (Lindberg Blue) located under a fume hood. The schematic of growth is shown in Figure 1. The furnaces were equipped with fused silica (quartz) tubes, while the furnace temperatures were monitored using the built-in furnace thermocouples. During the growth of the dichalcogenide (MoSe₂), the temperatures were set at 650 °C for the first furnace (F1) at the elemental Se side and 900 °C for the metal foil (i.e., Mo foil) for the second furnace (F2).^{23,25} All experiments were conducted under a steady flow of Argon gas (99.999%, from Gas Technologies). Before synthesis, each of the Mo foils was etched with dilute hydrochloric acid [with a variation in the concentration of the HCl being 0.0001, 0.001, 0.01, and 0.1 M]. A separate set of control metal foils was also taken, which were cleaned only with isopropanol. The final product showed a variable coating color on the etched Mo foil's exposed surface, indicating that the metal foil's surface reacted with the elemental Se, leading to the TMDC. We observed that this TMDC formed at identical temperatures and reaction conditions compared to our previously reported 2H-WSe₂. This indicates that our process adapted from the previous study is highly reproducible with consistently repeatable results.²³

Exfoliation of Bulk Molybdenum Selenide (2H-MoSe₂) Synthesized on the Mo Foil Surface. We previously studied the solvents responsible for the proper exfoliation of 2D layered transition-metal selenides.^{24,26} The polarity of these solvents seems to dictate the layers' overall separation after drop-casting them on suitable substrates. In this regard, liquid-phase exfoliation (LPE) with low boiling point solvents such as ethanol or isopropanol efficiently leads to layered nanosheets in their respective liquid dispersions (and sometimes in the presence of an additive of stabilizer). LPE is primarily based on solubility parameters. Ideally, any 2D layered material can be taken and immersed in a suitable solvent chosen based on its surface energy. The energy is

supplied to the system through sonication. It must be greater or equal to the material surface energy to overcome the van der Waals interactions between the layers in bulk. When sufficient energy is provided, layer separation occurs, and a range of layered nanosheets are dispersed in the solvent. Also, quantitatively speaking, the method can be scaled up easily. The as-prepared bulk molybdenum selenide (2H-MoSe₂) was dispersed and then exfoliated into few-layer nanosheets using the liquid-phase exfoliation (LPE) method after dispersing the bulk samples in ethanol (50 mL, purchased from Romical). We sonicated the dispersions for different durations. We obtained the most uniform homogeneous dispersion after 60 min. All exfoliation studies were done at room temperature in a frequency variable ultrasonic bath (Elmasonic P) (we chose 80 kHz frequency and 100 W power). All of the prepared dispersions were dried and used for separate analyses. Some of the dispersions were drop-cast on Si/SiO₂ wafers and CaF₂ to determine the LFR Raman spectra and perform subsequent analyses (e.g., AFM measurements of the number of layers).

CHARACTERIZATION

Physical Characterization. The X-ray diffraction measurements of the bulk molybdenum diselenide (MoSe₂) grown on the molybdenum (Mo) foil are performed using a Rigaku SmartLab X-ray diffractometer. We analyzed a 2 cm × 2 cm sample of bulk molybdenum diselenide (MoSe₂). The data are collected in the 2θ range from 20 to 70°, with a step size of 0.004° and a scanning rate of 0.4°/min. The X-ray generator is operated at 40 kV and 30 mA with Cu Kα radiation (λ = 1.542 Å). The crystallinity and purity of the as-synthesized molybdenum diselenide (MoSe₂) on the molybdenum (Mo) foil were further analyzed by DiffracEva software for proper identification of the corresponding peaks in the XRD. High-resolution scanning electron microscopy (HRSEM) was done using a Magellan 400 FEI (for bulk MoSe₂). Additional examinations of the exfoliated flakes of MoSe₂ with atomic force microscopy (AFM) measurements were done using a Bio Fast Scan scanning probe microscope (Bruker AXS). All images were obtained using PeakForce QNM (PeakForce Quantitative Nanomechanical Mapping) mode with a FastScan-C (Bruker) silicon probe (spring constant of 0.45 N/m). The measurements were performed under environmental conditions in the acoustic hood to minimize vibrational noise. The images (retracing) are obtained with a resolution of about 512 samples/line. Nanoscope Analysis software was used with the "flattening" and "plane fit" functions applied to each image. We carried out an HRTEM of the samples in a JEOL, JEM 2100 (operating at 200 keV). HRTEM image analyses are done using Gatan Digital Micrograph. X-ray photoelectron spectroscopy (XPS) measurements are done using the Thermo Scientific Nexsa spectrometer with X-ray source (1.5 keV) under ultrahigh vacuum conditions (10⁻¹⁰ to 10⁻⁹ torr). At the same time, their ejected photoelectrons were analyzed, and the graphs were deconvoluted.

All Raman measurements were taken using a lab-built micro-Raman setup. The Raman-grade CaF₂ was purchased from Crystan, UK. The samples were excited using a single-mode laser excitation of 532 nm and 20 mW of optical power, which was integrated into an upright microscope (Olympus, BXFM) for reflective geometry measurements. The output scattering from the sample, which contained both Rayleigh and Raman signals, was routed into a specialized optical blocking filter system (ONDAX, XLFMICRO) consisting of three narrow-

band volume holographic notch filters to block laser light and intense Rayleigh scattering, with OD > 9 rejection ratio, from entering into the spectrometer. The blocking filters' output was fiber-coupled into an imaging spectrometer (Princeton Instruments, SP-2500i) and measured using an acquisition time of 30 s and a grating groove density of 1800 g/mm, with an electron-multiplying charge-coupled device camera (Princeton Instruments, Pro-EM: 16002).

Raman Study of 2H-MoSe₂ on CaF₂ Substrate Computational Details. The Raman intensity calculations were performed using density functional perturbation theory as implemented in the Quantum ESPRESSO code with norm-conserving pseudopotentials.^{45–47} The local density approximation (LDA) for the exchange–correlation functional is used. The kinetic energy cutoff for the wave functions was set to 100 Ry. The layered structures were made from their bulk parent structures. To avoid the interaction between periodic images, the vacuum length was more than 20 Å for all of the layered structures. The semiempirical method developed by Grimme⁴⁸ was used to include the van der Waals (vdW) interaction. In the ionic force minimization, the convergence criterion for each ion was set to 0.0001 au. The Brillouin zone integration was performed using the 10 × 10 × 1 *k*-mesh with the Monkhorst-Pack sampling scheme.

■ ASSOCIATED CONTENT

SI Supporting Information

The Supporting Information is available free of charge at <https://pubs.acs.org/doi/10.1021/acsomega.1c05652>.

Growth progression of bulk sheetlike MoSe₂; surface etching of Mo foils at different HCl strengths; growth mechanism of variable morphologies on etched Mo foils; HRSEM images of growth progression of other microstructures of MoSe₂; TEM, HRTEM, SAED, HRSEM, XRD, and XPS characterization of sheetlike MoSe₂ (0.01 M HCl etching procedure); elemental mapping, EDS, HRTEM of other regions in exfoliated sheetlike 2H-MoSe₂ (0.01 M HCl etching procedure); HRSEM of micromechanically exfoliated layers of sheetlike 2H-MoSe₂ (0.01 M HCl etching procedure); AFM images with height profiles of all exfoliated MoSe₂ morphologies; photograph of three different concentrations of sheetlike MoSe₂ dispersions (0.01 M HCl etching procedure, photograph taken by R.K.); Raman spectra of CaF₂ and Si/SiO₂ substrates; comparison of the slopes of laser power vs the intensity for the Raman-grade CaF₂ substrate and SiO₂/Si substrates; optical images of MoSe₂ sheets on CaF₂; effect of focus on MoSe₂ sheets (0.01 M HCl etching procedure) drop-cast on CaF₂; XRD of the bare CaF₂ substrate; and photoluminescence spectra of 2H-MoSe₂ sheets (0.01 M HCl etching procedure) (PDF)

■ AUTHOR INFORMATION

Corresponding Authors

Ilya Grinberg – Department of Chemistry and Institute of Nanotechnology, Bar-Ilan University, Ramat Gan 5290002, Israel; Email: ilya.grinberg@biu.ac.il

Yaakov Raphael Tischler – Department of Chemistry and Institute of Nanotechnology, Bar-Ilan University, Ramat Gan 5290002, Israel; orcid.org/0000-0001-8016-538X; Email: yrt@biu.ac.il

Gilbert Daniel Nessim – Department of Chemistry and Institute of Nanotechnology, Bar-Ilan University, Ramat Gan 5290002, Israel; orcid.org/0000-0003-0738-5436; Email: gilbert.nessim@biu.ac.il

Authors

Rajashree Konar – Department of Chemistry and Institute of Nanotechnology, Bar-Ilan University, Ramat Gan 5290002, Israel; orcid.org/0000-0003-2938-5541

Bharathi Rajeswaran – Department of Chemistry and Institute of Nanotechnology, Bar-Ilan University, Ramat Gan 5290002, Israel

Atanu Paul – Department of Chemistry and Institute of Nanotechnology, Bar-Ilan University, Ramat Gan 5290002, Israel

Eti Teblum – Department of Chemistry and Institute of Nanotechnology, Bar-Ilan University, Ramat Gan 5290002, Israel

Hagit Aviv – Department of Chemistry and Institute of Nanotechnology, Bar-Ilan University, Ramat Gan 5290002, Israel

Ilana Perelshtein – Department of Chemistry and Institute of Nanotechnology, Bar-Ilan University, Ramat Gan 5290002, Israel

Complete contact information is available at:

<https://pubs.acs.org/10.1021/acsomega.1c05652>

Author Contributions

[†]R.K. and B.R. equally contributed.

Author Contributions

R.K.: conceptualization, writing-original draft, formal analysis, writing, and editing; B.R.: methodology; A.P.: computational analysis; E.T.: methodology; H.A.: project administration; I.P.: methodology; I.G.: supervision; Y.R.T.: resources, supervision; and G.D.N.: investigation, resources, funding acquisition.

Notes

The authors declare no competing financial interest.

■ ACKNOWLEDGMENTS

G.D.N., Y.R.T., and I.G. are thankful for the Israel Ministry of Science and Technology (M.O.S.T.) Optoelectronics Grant (205509), titled “Compact monolithic wavelength-tunable microcavity diode laser based on electro-optic phase modulation using 2D nanomaterial thin films”, for funding of this study.

■ REFERENCES

- (1) Mas-Ballesté, R.; Gómez-Navarro, C.; Gómez-Herrero, J.; Zamora, F. 2D Materials: To Graphene and Beyond. *Nanoscale* **2011**, *3*, 20–30.
- (2) Zundel, L.; Manjavacas, A. Spatially Resolved Optical Sensing Using Graphene Nanodisk Arrays. *ACS Photonics* **2017**, *4*, 1831–1838.
- (3) Guo, Y.; Liu, C.; Yin, Q.; Wei, C.; Lin, S.; Hoffman, T. B.; Zhao, Y.; Edgar, J. H.; Chen, Q.; Lau, S. P.; Dai, J.; Yao, H.; Wong, H.-S. P.; Chai, Y. Distinctive In-Plane Cleavage Behaviors of Two-Dimensional Layered Materials. *ACS Nano* **2016**, *10*, 8980–8988.
- (4) Dresselhaus, M. S.; Jorio, A.; Hofmann, M.; Dresselhaus, G.; Saito, R. Perspectives on Carbon Nanotubes and Graphene Raman Spectroscopy. *Nano Lett.* **2010**, *10*, 751–758.
- (5) Aretouli, K. E.; Tsoutsou, D.; Tsiapas, P.; Marquez-Velasco, J.; Aministragia Giamini, S.; Kelaidis, N.; Psycharis, V.; Dimoulas, A. Epitaxial 2D SnSe₂/2D WSe₂ van Der Waals Heterostructures. *ACS Appl. Mater. Interfaces* **2016**, *8*, 23222–23229.

- (6) Tang, H.-L.; Chiu, M.-H.; Tseng, C.-C.; Yang, S.-H.; Hou, K.-J.; Wei, S.-Y.; Huang, J.-K.; Lin, Y.-F.; Lien, C.-H.; Li, L.-J. Multilayer Graphene–WSe₂ Heterostructures for WSe₂ Transistors. *ACS Nano* **2017**, *11*, 12817–12823.
- (7) Jeong, T. Y.; Jin, B. M.; Rhim, S. H.; Debbichi, L.; Park, J.; Jang, Y. D.; Lee, H. R.; Chae, D.-H.; Lee, D.; Kim, Y.-H.; Jung, S.; Yee, K. J. Coherent Lattice Vibrations in Mono- and Few-Layer WSe₂. *ACS Nano* **2016**, *10*, 5560–5566.
- (8) Wang, L.; Jie, J.; Shao, Z.; Zhang, Q.; Zhang, X.; Wang, Y.; Sun, Z.; Lee, S.-T. MoS₂/Si Heterojunction with Vertically Standing Layered Structure for Ultrafast, High-Detectivity, Self-Driven Visible-Near Infrared Photodetectors. *Adv. Funct. Mater.* **2015**, *25*, 2910–2919.
- (9) Liang, L.; Zhang, J.; Sumpter, B. G.; Tan, Q.-H.; Tan, P.-H.; Meunier, V. Low-Frequency Shear and Layer-Breathing Modes in Raman Scattering of Two-Dimensional Materials. *ACS Nano* **2017**, *11*, 11777–11802.
- (10) Lu, X.; Utama, M. I. B.; Lin, J.; Gong, X.; Zhang, J.; Zhao, Y.; Pantelides, S. T.; Wang, J.; Dong, Z.; Liu, Z.; Zhou, W.; Xiong, Q. Large-Area Synthesis of Monolayer and Few-Layer MoSe₂ Films on SiO₂ Substrates. *Nano Lett.* **2014**, *14*, 2419–2425.
- (11) Lui, C. H.; Malard, L. M.; Kim, S.; Lantz, G.; Laverge, F. E.; Saito, R.; Heinz, T. F. Observation of Layer-Breathing Mode Vibrations in Few-Layer Graphene through Combination Raman Scattering. *Nano Lett.* **2012**, *12*, 5539–5544.
- (12) Kerr, L. T.; Byrne, H. J.; Hennelly, B. M. Optimal Choice of Sample Substrate and Laser Wavelength for Raman Spectroscopic Analysis of Biological Specimen. *Anal. Methods* **2015**, *7*, S041–S052.
- (13) Wen, C.; Banschikov, A. G.; Illarionov, Y. Y.; Frammelsberger, W.; Knobloch, T.; Hui, F.; Sokolov, N. S.; Grasser, T.; Lanza, M. Dielectric Properties of Ultrathin CaF₂ Ionic Crystals. *Adv. Mater.* **2020**, *32*, No. 2002525.
- (14) Alessandri, I.; Lombardi, J. R. Enhanced Raman Scattering with Dielectrics. *Chem. Rev.* **2016**, *116*, 14921–14981.
- (15) Holler, J.; Meier, S.; Kempf, M.; Nagler, P.; Watanabe, K.; Taniguchi, T.; Korn, T.; Schüller, C. Low-Frequency Raman Scattering in WSe₂–MoSe₂ Heterobilayers: Evidence for Atomic Reconstruction. *Appl. Phys. Lett.* **2020**, *117*, No. 013104.
- (16) Gupta, U.; Naidu, B. S.; Maitra, U.; Singh, A.; Shirodkar, S. N.; Waghmare, U. V.; Rao, C. N. R. Characterization of Few-Layer 1T-MoSe₂ and Its Superior Performance in the Visible-Light Induced Hydrogen Evolution Reaction. *APL Mater.* **2014**, *2*, No. 092802.
- (17) Fu, X.; Li, F.; Lin, J.-F.; Gong, Y.; Huang, X.; Huang, Y.; Han, B.; Zhou, Q.; Cui, T. Pressure-Dependent Light Emission of Charged and Neutral Excitons in Monolayer MoSe₂. *J. Phys. Chem. Lett.* **2017**, *8*, 3556–3563.
- (18) Xia, J.; Huang, X.; Liu, L.-Z.; Wang, M.; Wang, L.; Huang, B.; Zhu, D.-D.; Li, J.-J.; Gu, C.-Z.; Meng, X.-M. CVD Synthesis of Large-Area, Highly Crystalline MoSe₂ Atomic Layers on Diverse Substrates and Application to Photodetectors. *Nanoscale* **2014**, *6*, 8949–8955.
- (19) Choi, W.; Choudhary, N.; Han, G. H.; Park, J.; Akinwande, D.; Lee, Y. H. Recent Development of Two-Dimensional Transition Metal Dichalcogenides and Their Applications. *Mater. Today* **2017**, *20*, 116–130.
- (20) Huang, Y.; Sutter, E.; Shi, N. N.; Zheng, J.; Yang, T.; Englund, D.; Gao, H.-J.; Sutter, P. Reliable Exfoliation of Large-Area High-Quality Flakes of Graphene and Other Two-Dimensional Materials. *ACS Nano* **2015**, *9*, 10612–10620.
- (21) Ottaviano, L.; Pallechi, S.; Perrozzi, F.; D'Olimpio, G.; Priante, F.; Donarelli, M.; Benassi, P.; Nardone, M.; Gonchigsuren, M.; Gombosuren, M.; Lucia, A.; Moccia, G.; Cacioppo, O. A. Mechanical Exfoliation and Layer Number Identification of MoS₂ Revisited. *2D Mater.* **2017**, *4*, No. 045013.
- (22) Huang, Y.; Pan, Y.-H.; Yang, R.; Bao, L.-H.; Meng, L.; Luo, H.-L.; Cai, Y.-Q.; Liu, G.-D.; Zhao, W.-J.; Zhou, Z.; Wu, L.-M.; Zhu, Z.-L.; Huang, M.; Liu, L.-W.; Liu, L.; Cheng, P.; Wu, K.-H.; Tian, S.-B.; Gu, C.-Z.; Shi, Y.-G.; Guo, Y.-F.; Cheng, Z. G.; Hu, J.-P.; Zhao, L.; Yang, G.-H.; Sutter, E.; Sutter, P.; Wang, Y.-L.; Ji, W.; Zhou, X.-J.; Gao, H.-J. Universal Mechanical Exfoliation of Large-Area 2D Crystals. *Nat. Commun.* **2020**, *11*, No. 2453.
- (23) Konar, R.; Rosy; Perelshtein, I.; Teblum, E.; Telkhozhayeva, M.; Tkachev, M.; Richter, J. J.; Cattaruzza, E.; Pietropolli Charmet, A.; Stoppa, P.; Noked, M.; Nessim, G. D. Scalable Synthesis of Few-Layered 2D Tungsten Diselenide (2H-WSe₂) Nanosheets Directly Grown on Tungsten (W) Foil Using Ambient-Pressure Chemical Vapor Deposition for Reversible Li-Ion Storage. *ACS Omega* **2020**, *5*, 19409–19421.
- (24) Moumen, A.; Konar, R.; Zappa, D.; Teblum, E.; Perelshtein, I.; Lavi, R.; Ruthstein, S.; Nessim, G. D.; Comini, E. Robust Room-Temperature NO₂ Sensors from Exfoliated 2D Few-Layered CVD-Grown Bulk Tungsten Di-Selenide (2H-WSe₂). *ACS Appl. Mater. Interfaces* **2021**, *13*, 4316–4329.
- (25) Konar, R.; Das, S.; Teblum, E.; Modak, A.; Perelshtein, I.; Richter, J. J.; Schechter, A.; Nessim, G. D. Facile and Scalable Ambient Pressure Chemical Vapor Deposition-Assisted Synthesis of Layered Silver Selenide (β -Ag₂Se) on Ag Foil as a Possible Oxygen Reduction Catalyst in Alkaline Medium. *Electrochim. Acta* **2021**, *370*, No. 137709.
- (26) Telkhozhayeva, M.; Teblum, E.; Konar, R.; Girshevit, O.; Perelshtein, I.; Aviv, H.; Tischler, Y. R.; Nessim, G. D. Higher Ultrasonic Frequency Liquid Phase Exfoliation Leads to Larger and Monolayer to Few-Layer Flakes of 2D Layered Materials. *Langmuir* **2021**, *37*, 4504–4514.
- (27) Xia, C.; Alshareef, H. N. Self-Templating Scheme for the Synthesis of Nanostructured Transition-Metal Chalcogenide Electrodes for Capacitive Energy Storage. *Chem. Mater.* **2015**, *27*, 4661–4668.
- (28) Yun, Q.; Li, L.; Hu, Z.; Lu, Q.; Chen, B.; Zhang, H. Layered Transition Metal Dichalcogenide-Based Nanomaterials for Electrochemical Energy Storage. *Adv. Mater.* **2020**, *32*, No. 1903826.
- (29) Chacham, H.; Santos, J. C. C.; Pacheco, F. G.; Silva, D. L.; Martins, R. M.; Del'Boccio, J. P.; Soares, E. M.; Altoé, R.; Furtado, C. A.; Plentz, F.; Neves, B. R. A.; Cançado, L. G. Controlling the Morphology of Nanoflakes Obtained by Liquid-Phase Exfoliation: Implications for the Mass Production of 2D Materials. *ACS Appl. Nano Mater.* **2020**, *3*, 12095–12105.
- (30) Mayerhöfer, T. G.; Pahlow, S.; Hübner, U.; Popp, J. CaF₂: An Ideal Substrate Material for Infrared Spectroscopy? *Anal. Chem.* **2020**, *92*, 9024–9031.
- (31) Gasparov, L.; Jegorel, T.; Loetgering, L.; Middey, S.; Chakhalian, J. Thin Film Substrates from the Raman Spectroscopy Point of View. *J. Raman Spectrosc.* **2014**, *45*, 465–469.
- (32) Puzetzy, A. A.; Liang, L.; Li, X.; Xiao, K.; Wang, K.; Mahjouri-Samani, M.; Basile, L.; Idrobo, J. C.; Sumpter, B. G.; Meunier, V.; Geoghegan, D. B. Low-Frequency Raman Fingerprints of Two-Dimensional Metal Dichalcogenide Layer Stacking Configurations. *ACS Nano* **2015**, *9*, 6333–6342.
- (33) Zheng, H.; Liu, Y.; Lin, H.; Liu, B.; Gu, X.; Li, D.; Huang, B.; Wu, Y.; Dong, L.; Zhu, W.; Tang, J.; Guan, H.; Lu, H.; Zhong, Y.; Fang, J.; Luo, Y.; Zhang, J.; Yu, J.; Chen, Z.; Tittel, F. K. Quartz-Enhanced Photoacoustic Spectroscopy Employing Pilot Line Manufactured Custom Tuning Forks. *Photoacoustics* **2020**, *17*, No. 100158.
- (34) Dutta, J.; Anantha Ramakrishna, S.; Lakhtakia, A. Characteristics of Surface Plasmon–Polariton Waves Excited on 2D Periodically Patterned Columnar Thin Films of Silver. *J. Opt. Soc. Am.* **2016**, *33*, No. 1697.
- (35) Mahjouri-Samani, M.; Liang, L.; Oyedele, A.; Kim, Y.-S.; Tian, M.; Cross, N.; Wang, K.; Lin, M.-W.; Boulesbaa, A.; Rouleau, C. M.; Puzetzy, A. A.; Xiao, K.; Yoon, M.; Eres, G.; Duscher, G.; Sumpter, B. G.; Geoghegan, D. B. Tailoring Vacancies Far Beyond Intrinsic Levels Changes the Carrier Type and Optical Response in Monolayer MoSe_{2-x} Crystals. *Nano Lett.* **2016**, *16*, 5213–5220.
- (36) O'Brien, M.; McEvoy, N.; Hanlon, D.; Lee, K.; Gatensby, R.; Coleman, J. N.; Duesberg, G. S. Low Wavenumber Raman Spectroscopy of Highly Crystalline MoSe₂ Grown by Chemical Vapor Deposition. *Phys. Status Solidi B* **2015**, *252*, 2385–2389.

(37) O'Brien, M.; McEvoy, N.; Hanlon, D.; Hallam, T.; Coleman, J. N.; Duesberg, G. S. Mapping of Low-Frequency Raman Modes in CVD-Grown Transition Metal Dichalcogenides: Layer Number, Stacking Orientation and Resonant Effects. *Sci. Rep.* **2016**, *6*, No. 19476.

(38) Zhang, X.; Qiao, X.-F.; Shi, W.; Wu, J.-B.; Jiang, D.-S.; Tan, P.-H. Phonon and Raman Scattering of Two-Dimensional Transition Metal Dichalcogenides from Monolayer, Multilayer to Bulk Material. *Chem. Soc. Rev.* **2015**, *44*, 2757–2785.

(39) Roy, A.; Movva, H. C. P.; Satpati, B.; Kim, K.; Dey, R.; Rai, A.; Pramanik, T.; Guchhait, S.; Tutuc, E.; Banerjee, S. K. Structural and Electrical Properties of MoTe₂ and MoSe₂ Grown by Molecular Beam Epitaxy. *ACS Appl. Mater. Interfaces* **2016**, *8*, 7396–7402.

(40) Nam, D.; Lee, J.-U.; Cheong, H. Excitation Energy Dependent Raman Spectrum of MoSe₂. *Sci. Rep.* **2015**, *5*, No. 17113.

(41) Zhao, S.; Lu, M.; Xue, S.; Yan, L.; Miao, P.; Hang, Y.; Wang, X.; Liu, Z.; Wang, Y.; Tao, L.; Sui, Y.; Wang, Y. A Se Vacancy Induced Localized Raman Mode in Two-Dimensional MoSe₂ Grown by CVD. 2019, arXiv:1904.09789. arXiv.org e-Print archive. <http://arxiv.org/abs/1904.09789>.

(42) McDonnell, L. P.; Viner, J. J. S.; Rivera, P.; Xu, X.; Smith, D. C. Observation of Intravalley Phonon Scattering of 2s Excitons in MoSe₂ and WSe₂ Monolayers. *2D Mater.* **2020**, *7*, No. 045008.

(43) Soubelet, P.; Bruchhausen, A. E.; Fainstein, A.; Nogajewski, K.; Faugeras, C. Resonance Effects in the Raman Scattering of Monolayer and Few-Layer MoSe₂. *Phys. Rev. B* **2016**, *93*, No. 155407.

(44) Terrones, H.; Del Corro, E.; Feng, S.; Poumirol, J. M.; Rhodes, D.; Smirnov, D.; Pradhan, N. R.; Lin, Z.; Nguyen, M. A. T.; Elías, A. L.; Mallouk, T. E.; Balicas, L.; Pimenta, M. A.; Terrones, M. New First Order Raman-Active Modes in Few Layered Transition Metal Dichalcogenides. *Sci. Rep.* **2015**, *4*, No. 4215.

(45) Giannozzi, P.; Baroni, S.; Bonini, N.; Calandra, M.; Car, R.; Cavazzoni, C.; Ceresoli, D.; Chiarotti, G. L.; Cococcioni, M.; Dabo, I.; Dal Corso, A.; de Gironcoli, S.; Fabris, S.; Fratesi, G.; Gebauer, R.; Gerstmann, U.; Gougoussis, C.; Kokalj, A.; Lazzeri, M.; Martin-Samos, L.; Marzari, N.; Mauri, F.; Mazzarello, R.; Paolini, S.; Pasquarello, A.; Paulatto, L.; Sbraccia, C.; Scandolo, S.; Sclauzero, G.; Seitsonen, A. P.; Smogunov, A.; Umari, P.; Wentzcovitch, R. M. QUANTUM ESPRESSO: A Modular and Open-Source Software Project for Quantum Simulations of Materials. *J. Phys.: Condens. Matter* **2009**, *21*, No. 395502.

(46) Hamann, D. R. Optimized Norm-Conserving Vanderbilt Pseudopotentials. *Phys. Rev. B* **2013**, *88*, No. 085117.

(47) <http://www.pseudo-dojo.org/> (accessed 2022-01-13).

(48) Grimme, S. Semiempirical gga-type Density Functional Constructed with a Long-Range Dispersion Correction. *J. Comput. Chem.* **2006**, *27* (15), 1787–1799.